Electronic Supplementary Information

Electronic Structure Engineering of Bimetallic NiFe-MOF via One-Dimensional Tubular Assembly for Enhanced Oxygen Evolution

Bo Lin, Jun Zhang, Rui Wang, Fu-Hu Cao, Sheng Cheng, Ya-Rong Zheng,* Chuan-Ling Zhang*

Anhui Province Engineering Research Center of Flexible and Intelligent Materials, Anhui Province Key Laboratory of Value-Added Catalytic Conversion and Reaction Engineering, School of Chemistry and Chemical Engineering
Hefei University of Technology, Hefei 230009, China.
Email: yrzh@hfut.edu.cn; zhangcl@hfut.edu.cn

Experimental Section

Chemical and materials

Ferric chloride hexahydrate ($FeCl_3 \cdot 6H_2O$), Potassium hydroxide (KOH), Anhydrous ethanol, Polyacrylonitrile (PAN), purchased from Sinopharm Chemical Reagent Co., LTD, Nickel (II) nitrate hexahydrate ($Ni(NO_3)_2 \cdot 6H_2O$), purchased from Sigma-Aldrich. Terephthalic acid (H_2BDC), Nafion (5 wt%) purchased from Beijing Balingwei Technology Co., LTD. Nickel foam (NF) and carbon paper purchased from Sinero Technology Co., Ltd. Carbon black purchased from the Cabot Co., LTD. The solvent used in the experiments was 18.2 MΩ cm^{-2} of deionized water. All chemical reagents are used directly without further purification.

Experimental procedure

Synthesis of H_2BDC/PAN: Dissolve 1.08 g of H_2BDC in 20 mL of N,N-dimethylformamide (DMF) solution by ultrasonication for 5 minutes until completely dissolved. Next, add 1.5 g of PAN and stir at 25-30 °C for 20 hours (at 400 rpm) to prevent crystallization of the spinning solution, yielding a pale yellow solution. Transfer the spinning solution to a 10 mL syringe. Set the flow rate to 0.5 $mL \cdot h^{-1}$ and the DC voltage to 12.5 kV. Use a copper mesh as the receiving screen positioned approximately 15 cm from the needle tip. After 2 hours of continuous spinning, peel off to obtain a nanofiber membrane containing H_2BDC.

Synthesis of PAN@Ni_2Fe_1-MOFs: Place 0.29 g of $Ni(NO_3)_2 \cdot 6H_2O$ and 0.135 g of $FeCl_3 \cdot 6H_2O$ into a 40 mL reactor vessel. Add 30 mL of anhydrous ethanol and sonicate for 10 minutes. After complete dissolution of both metal salts, weigh 50 mg of H_2BDC/PAN fiber film and add it to the reactor. Place the reactor in a 150 °C oven and maintain the temperature for 3 hours. Then rinse three times with anhydrous ethanol and transfer to a 60 °C vacuum drying oven. After drying, PAN@Ni_2Fe_1-BDC are obtained.

Synthesis of Ni_2Fe_1-BDC NTs: Place the dried PAN@Ni_2Fe_1-BDC fiber films in DMF solution for 10 minutes to etch away the PAN. After centrifugation, wash three times with ethanol solution, then dry to obtain Ni_2Fe_1-BDC nanotubes.

For comparison, to investigate the effects of different components and their ratios on catalyst performance, under otherwise identical conditions, only $Ni(NO_3)_2 \cdot 6H_2O$ was added to the reactor to synthesize Ni-BDC nanotubes. When only $FeCl_3 \cdot 6H_2O$ was added, Fe-BDC NTs

were synthesized. By altering the molar ratio of nickel to iron metal salts to 1:1 and 3:1, Ni_1Fe_1-BDC NTs and Ni_3Fe_1-BDC NTs were prepared using the same methodology.

Characterization

The composition of the material and the internal structure of the crystals were analyzed by X-ray diffraction (XRD, PANalytical X-Pert PRO MPD); the test range was 5° to 80° and the sweep speed was 10° min^{-1}. The microstructure and composition of the samples were analyzed by scanning electron microscopy (SEM, SU8020) and transmission electron microscopy (TEM, HT-7700). X-ray photoelectron spectroscopy (XPS, TGL-10B) was used to discover chemical information on the surface of the sample. Analyze the pore size distribution, pore volume, and specific surface area of materials using Brunauer-Emmett-Teller Analyzer (BET, Autosorb-IQ). Determine the chemical composition and molecular structure of materials via Fourier Transform Infrared Spectroscopy (FT-IR, Bruker Invenio) and confocal laser micro-Raman spectroscopy (Raman, LABRAM-HRHORIBA JOBIN YVON). Inductively coupled plasma optical emission spectroscopy (ICP-OES) results were obtained using Agilent Technologies 7500 series. The results of the hydrophilicity test were obtained using a contact angle measuring instrument (POWEREACH). High-resolution transmission electron microscopy (HRTEM, Talos F 200 X G2) is employed to analyze the crystal structure of samples.

Electrochemical measurements

Electrochemical measurements were conducted at room temperature using a conventional three-electrode system on an electrochemical workstation (Autolab). Prior to testing, O_2 was bubbled into the electrolyte to achieve oxygen saturation. During testing, a graphite carbon rod served as the working electrode, a saturated Ag/AgCl electrode (with supersaturated KCl as the salt bridge) as the reference electrode, and a glassy carbon rotating disk electrode (RDE, 0.196 cm^2) as the counter electrode. A 1 M KOH aqueous solution was used as the alkaline electrolyte. The GC electrode was meticulously polished using 500 nm and 50 nm Al_2O_3 powders. The catalyst and carbon black were dispersed in a mixture of 5 wt% Nafion and 500 µL ethanol under ultrasonication. After 4 hours of ultrasonication, a uniform ink was formed. Subsequently, 15 µL of the catalyst ink was dispensed onto the glassy carbon electrode (GC) surface. After drying at room temperature, OER testing was conducted. To obtain stable and accurate test results, multiple cyclic voltammetry (CV) cycles were performed prior to linear

sweep voltammetry (LSV) curve testing. Subsequently, the working electrode rotation speed was set to 1600 rpm, and LSV curves were tested at 5 mV s^{-1} over a potential range of 0.0-1.0 V. All potential values obtained from this three-electrode system were converted to reversible hydrogen electrode (RHE) potentials using the following conversion formula:

$$E_{RHE} = E_{Ag/AgCl} + 0.059 \times pH + 0.198 \quad (1)$$

The calculation of overpotential for OER:

$$\eta = E_{RHE} - 1.23 \quad (2)$$

The Tafel plots were obtained from the LSV curves. The Tafel slope for OER was calculated by the equation below:

$$E = a + b * logj \quad (3)$$

C_{dl} was determined bymeasuring CVs with multiple scan rates in non-faradaic potentialregion. CV curves were measured at various scan rates from 20 to 100 mV·s^{-1}. The calculation formula of C_{dl} is: C_{dl} = Ic/v. C_{dl} in the equation isthe double layer capacitance (mF cm^{-2}), Ic is the charging current (mA cm^{-2}) and v is the scan rate (mV s^{-1}).Electrochemical impedance spectroscopy (EIS) was measured in thefrequency range from 100 kHz to 0.1 Hz in 1.0 M KOH solution. EIS measurements were performedat 1.5 V vs. RHE after activation.

In an alkaline medium, the overall OER process is accepted as $4OH^- \rightarrow O_2 + 2H_2O + 4e^-$,which involves four proton-transfer steps as follows:

$*+ OH^- \rightarrow * OH + e^-$

$* OH + OH^- \rightarrow * O + H_2O + e^-$

$* O + OH^- \rightarrow * OOH + e^-$

$* OOH + OH^- \rightarrow * O_2 + H_2O + e^-$

$* O_2 \rightarrow *+ O_2$

Electrocatalytic overall water splitting performances

The overall water splitting performance was evaluated using the two-electrode system. In a single-chamber electrolytic cell, a 100 µL slurry of electrocatalyst and 20 wt% Pt/C was dropped on the pretreated NF as anode and cathode, respectively (referred to as Ni_2Fe_1-BDC NTs||Pt/C). 20 wt% Pt/C||RuO_2 were prepared under the same condition for comparison.

Anion exchange membrane water electrolyzer (AEMWE) measurements

For anode preparation, a 2×2 cm^2 piece of nickel foam was sequentially sonicated for 10 minutes in 20% hydrochloric acid, methanol, and deionized water to remove surface impurities and oxides. It is then fixed on a vacuum heating platform at 60 °C. Catalyst ink is uniformly sprayed onto the NF surface using a spray gun, dried for 10 minutes, cooled to room temperature, and weighed. To achieve the target loading, multiple small-volume spraying and weighing steps are repeated until the catalyst loading density reaches 4 mg cm^{-2}.For the cathode, a commercial Pt/C catalyst was dispersed in a mixture of anhydrous ethanol and naphthol, ultrasonicated for 30 minutes to form a uniform ink. This ink was then loaded onto a 2×2 cm^2 carbon paper using the same spraying method, with loading controlled by weighing to achieve 0.5 mg cm^{-2}. A 2.2 × 2.2 cm^2 anion exchange membrane (PAW-1-60) was placed between the anode and cathode catalyst layers to assemble the Ni_2Fe_1-BDCNTs/NF||Pt/C/CP anion exchange membrane electrolyzer. During testing, 1.0 M KOH solution was continuously circulated at a flow rate of 10 mL/min to both sides of the electrolyzer.

Supplementary Figures and Tables

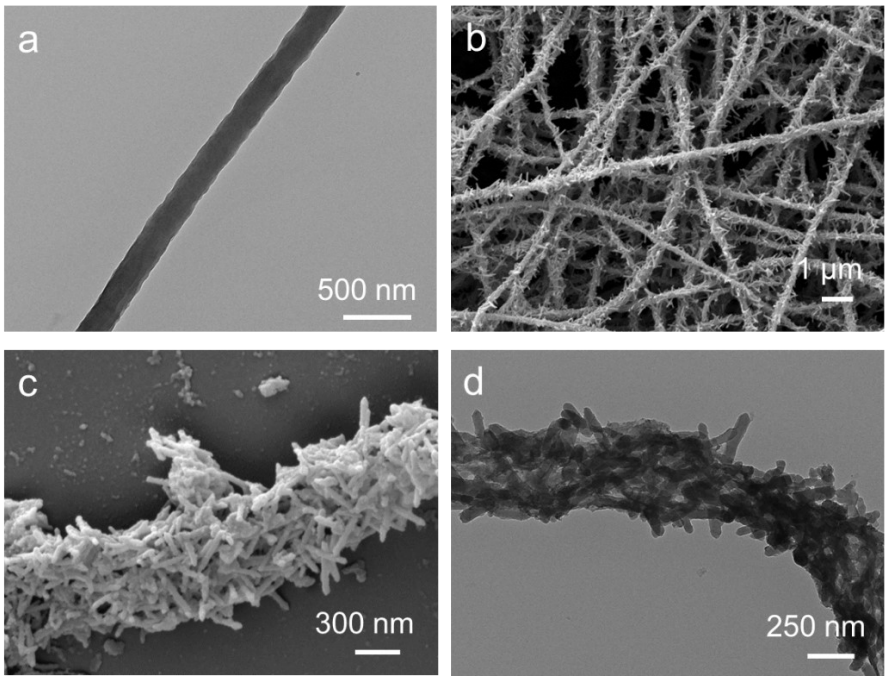

Figure S1. SEM images of (a) PAN/H_2BDC and (b) PAN@Ni_2Fe_1-BDC, (c) SEM image and (d) TEM image of Ni_2Fe_1-BDC NTs.

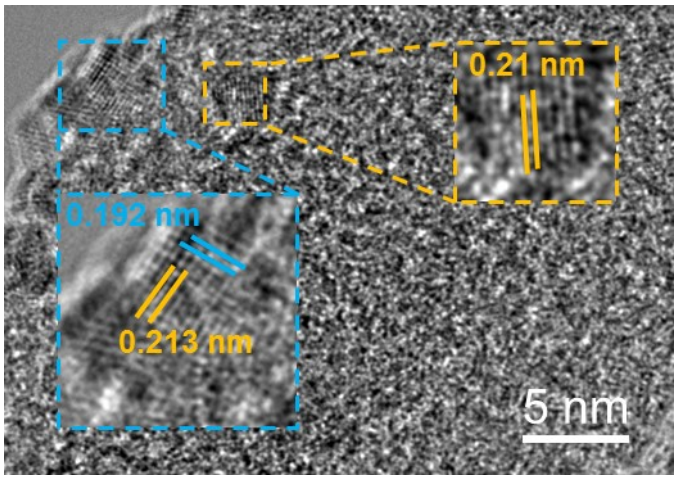

Figure S2. HRTEM image of Ni_2Fe_1-BDC NTs.

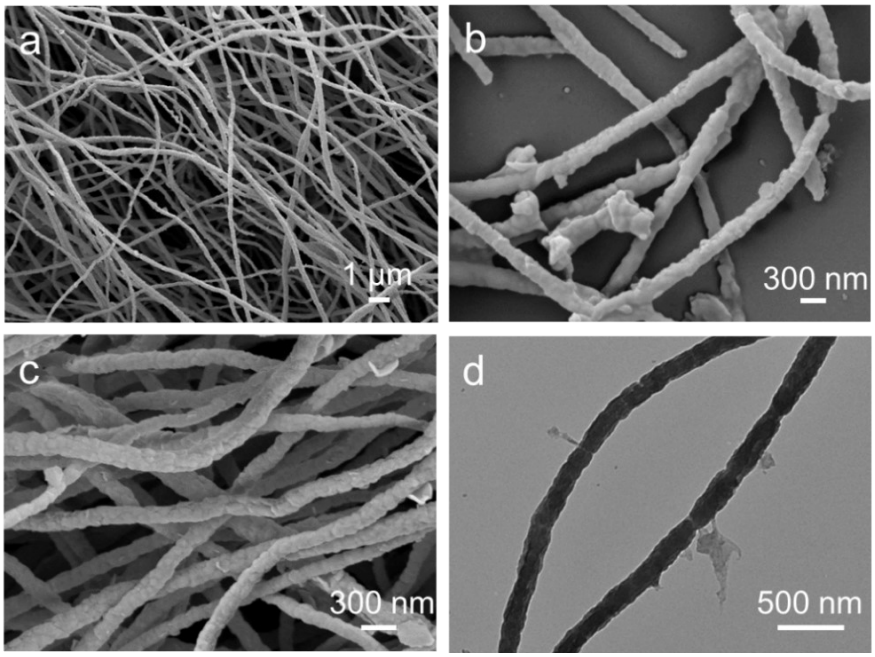

Figure S3. (a, c) SEM images of PAN@Ni-BDC, (b) SEM image and (d) TEM image of Ni-BDC NTs.

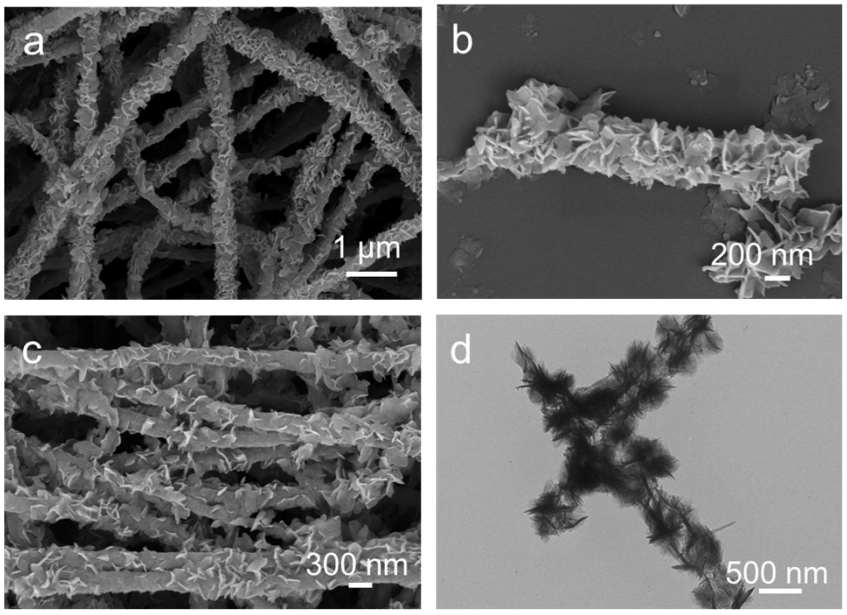

Figure S4. (a, c) SEM images of PAN@Fe-BDC, (b) SEM image and (d) TEM image of Fe-BDC NTs.

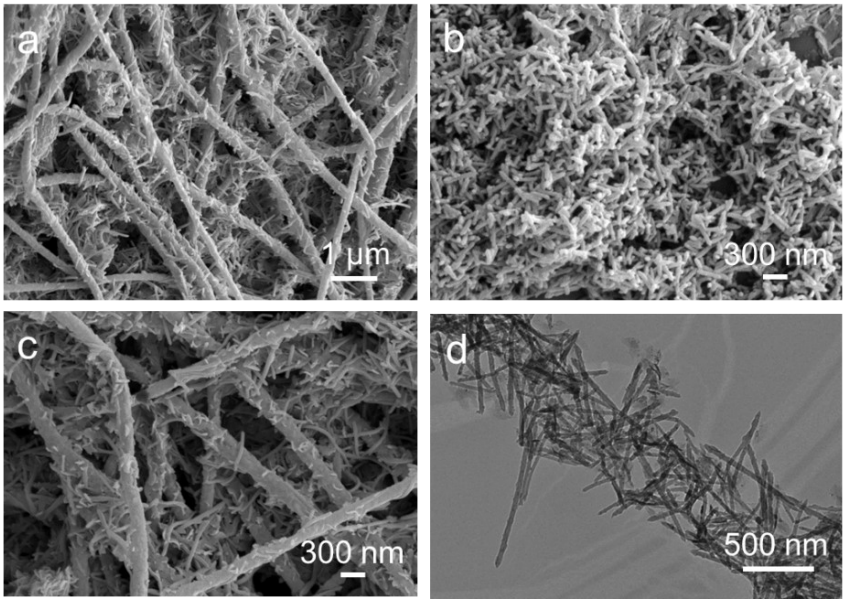

Figure S5. (a, c) SEM images of PAN@Ni_1Fe_1-BDC, (b) SEM image and (d) TEM image of Ni_1Fe_1-BDC NTs.

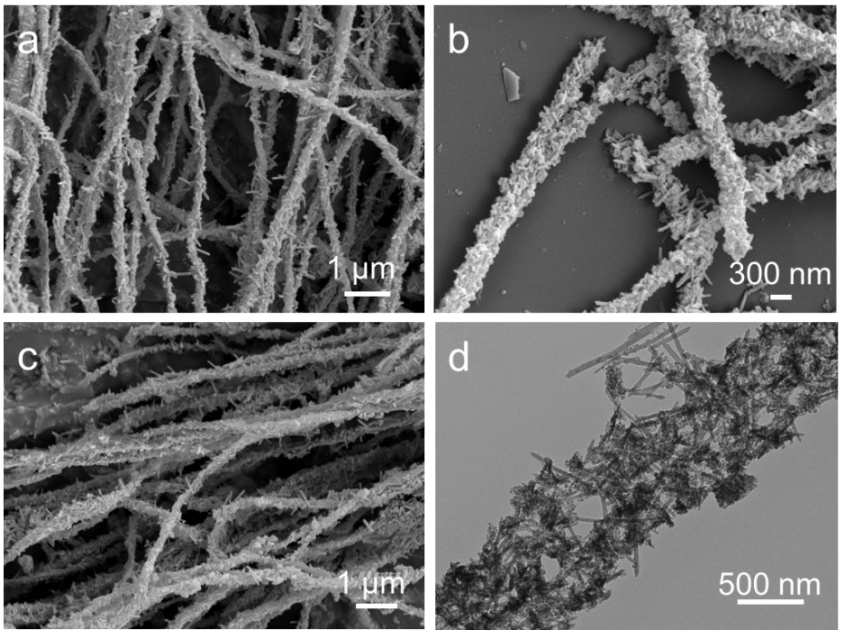

Figure S6. (a, c) SEM images of PAN@Ni_3Fe_1-BDC, (b) SEM image and (d) TEM image of Ni_3Fe_1-BDC NTs.

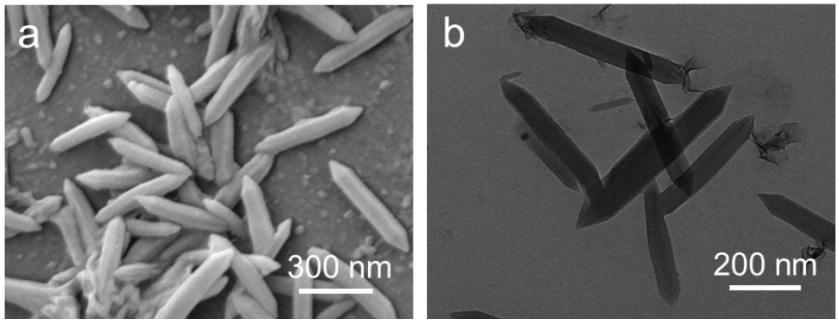

Figure S7. (a) SEM and (b) TEM images of Ni_2Fe_1-BDC.

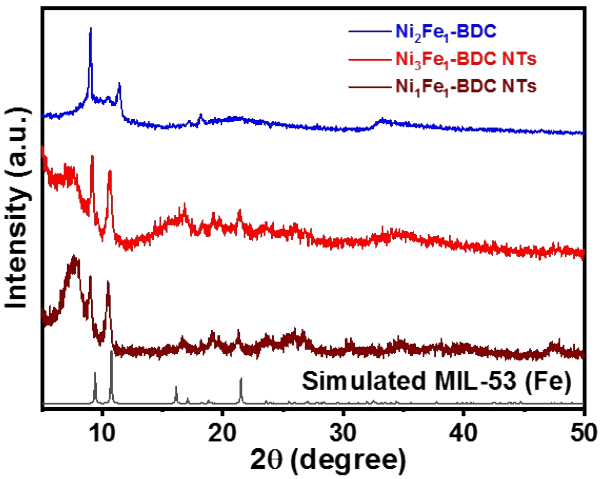

Figure S8. XRD patterns of Ni_2Fe_1-BDC, Ni_1Fe_1-BDC NTs and Ni_3Fe_1-BDC NTs.

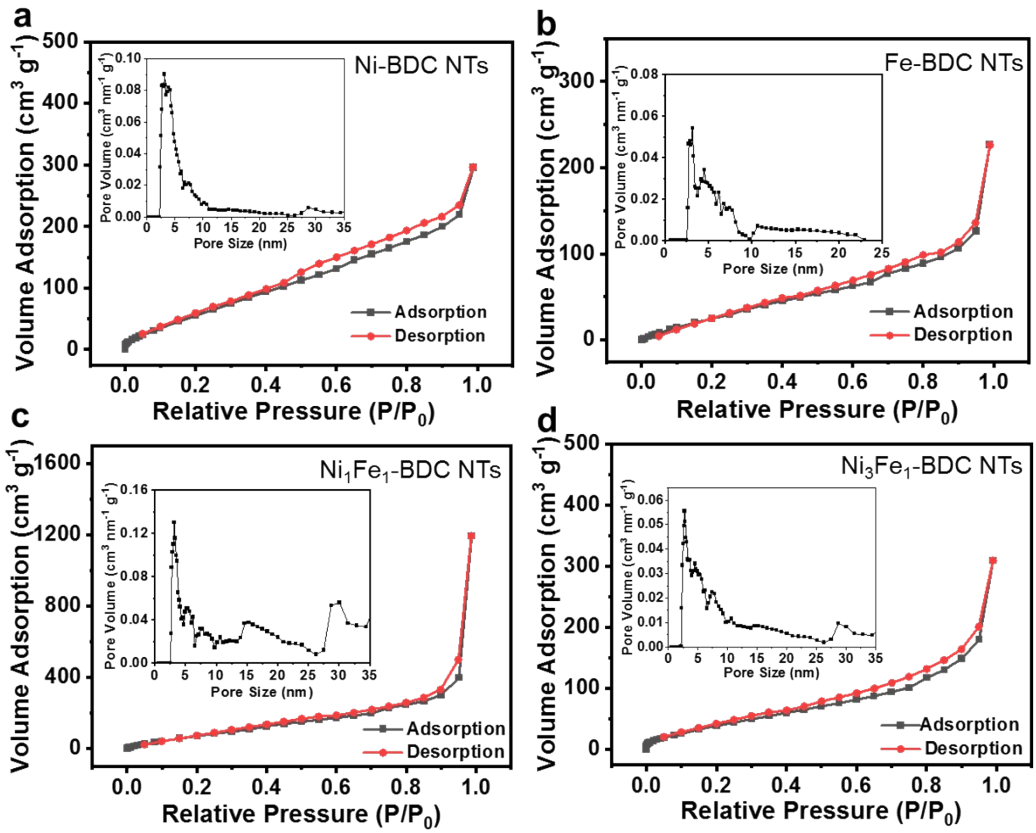

Figure S9. N_2 sorption isotherms of as-prepared samples and insets are the corresponding pore size distribution curves.

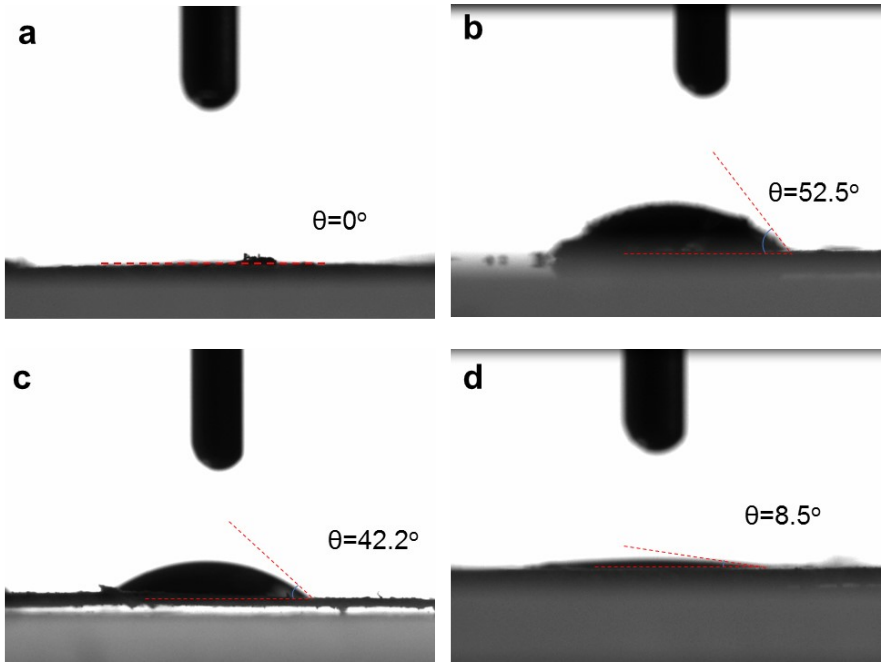

Figure S10. Contact angle measurements of (a) Ni_2Fe_1-BDC NTs, (b) Fe-BDC NTs, (c) Ni-BDC NTs, and (d) Ni_2Fe_1-BDC, respectively.

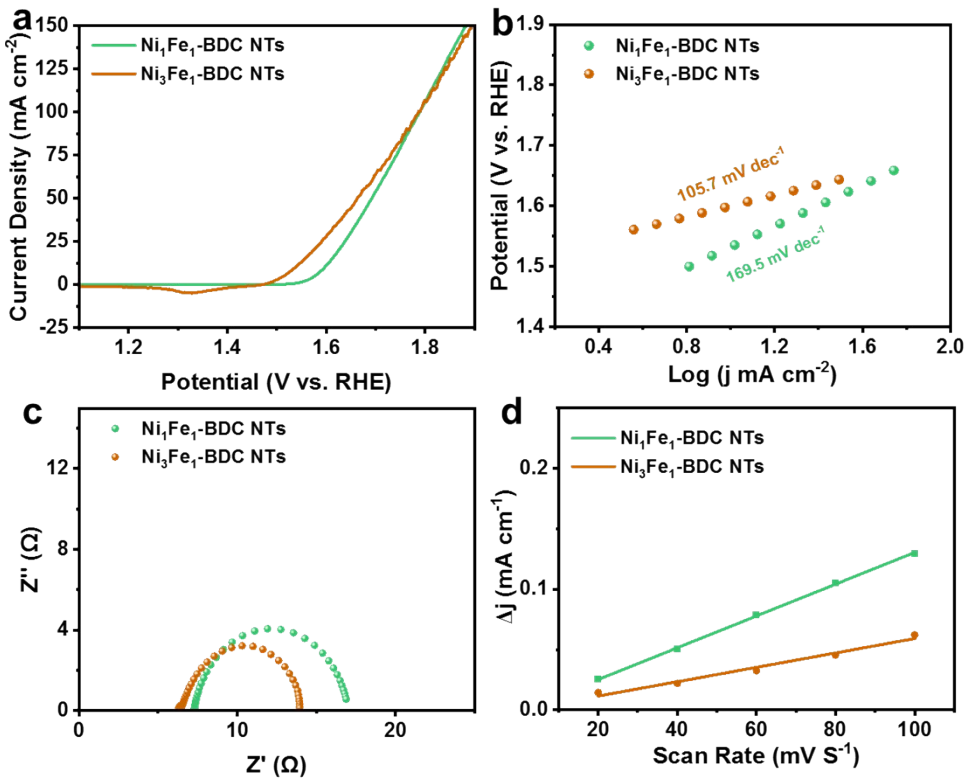

Figure S11. The electrochemical measurements of the samples in 1 M KOH saturated with O_2. (a) LSV curves, (b) Tafel slope diagram corresponding to (a), (c) Electrochemical impedance spectra (EIS), (d) linear relationship of the current density difference values against the scan rates.

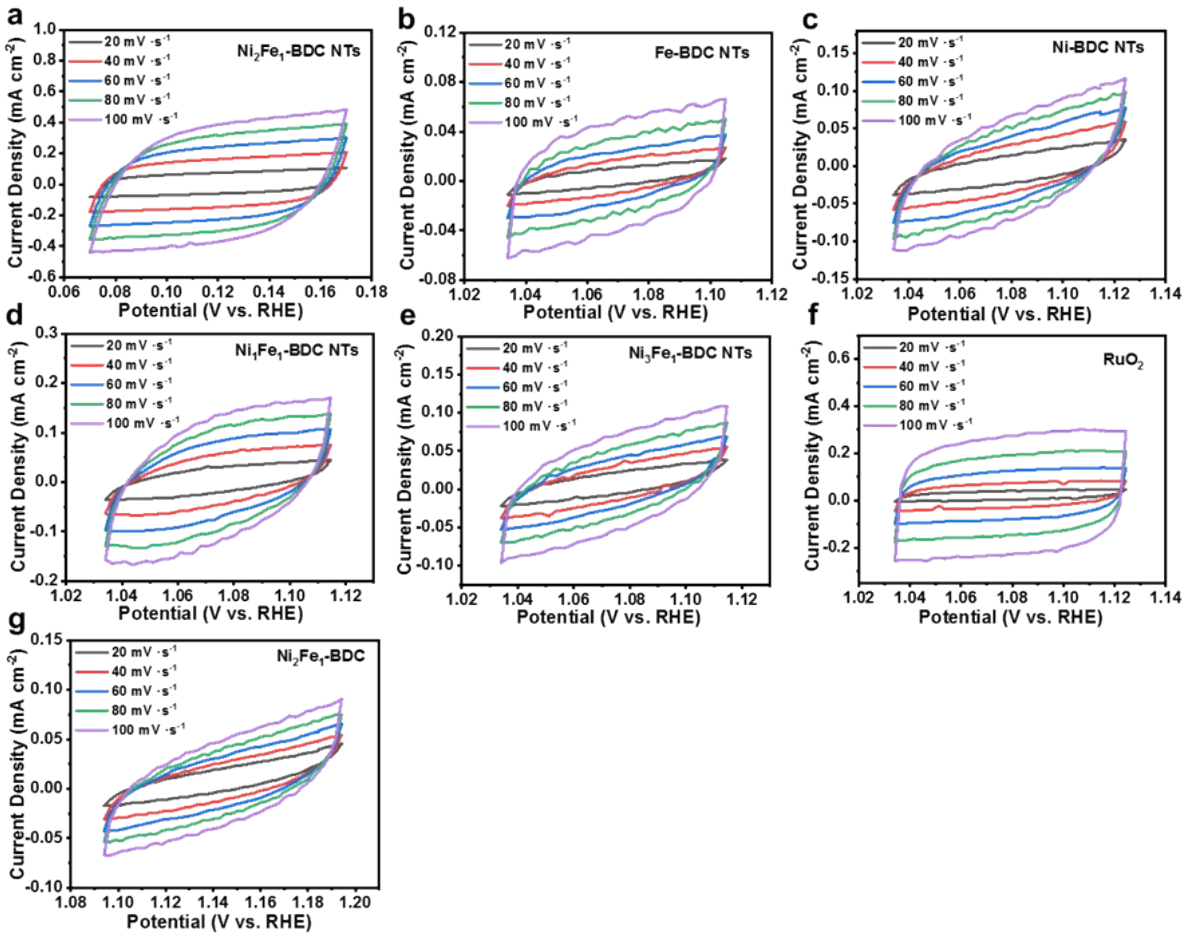

Figure S12. CV curves of each sample at different scanning speeds: (a) Ni_2Fe_1-BDC NTs, (b) Fe-BDC NTs, (c) Ni-BDC NTs, (d) Ni_1Fe_1-BDC NTs, (e) Ni_3Fe_1-BDC NTs, (f) RuO_2, (g) Ni_2Fe_1-BDC.

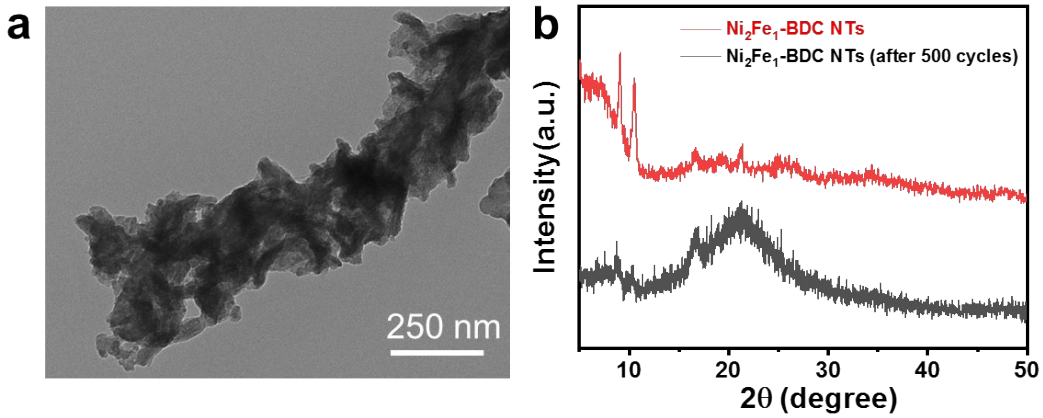

Figure S13. (a) TEM image of Ni_2Fe_1-BDC NTs after 500 CV cycles, (b) XRD patterns of Ni_2Fe_1-BDC NTs before and after 500 CV cycles.

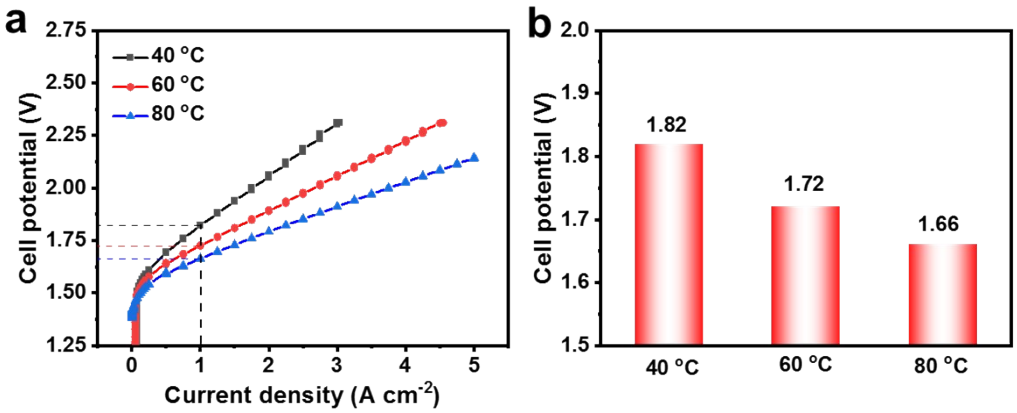

Figure S14. (a) Polarization curves of the Ni_2Fe_1-BDC NTs||Pt/C in the AEMWE at various temperatures, (b) voltage values corresponding to a current density of 1 A cm^{-2} at various temperatures in Figure (a).

Table S1. The specific surface area and total pore volume of the samples.

Catalyst	Surface area ($m^2 \cdot g^{-1}$)	Total pore volume ($cm^3 \cdot g^{-1}$)
Ni_1Fe_1-BDC NTs	**209.87**	**1.09**
Ni_2Fe_1-BDC NTs	**145.48**	**0.43**
Ni_3Fe_1-BDC NTs	**102.28**	**0.36**
Ni-BDC NTs	**128.45**	**0.38**
Fe-BDC NTs	**69.88**	**0.19**

Table S2. The metal content of Ni and Fe in these samples.

Catalyst	Ni (% mass)	Fe (% mass)
Ni_1Fe_1-BDC NTs	**5.1**	**27.1**
Ni_2Fe_1-BDC NTs	**11.9**	**20.6**
Ni_3Fe_1-BDC NTs	**14.9**	**11.5**

Table S3. The C_{dl} of the electrocatalysts prepared in this work.

Electrocatalyst	C_{dl} ($mF\ cm^{-2}$)
Fe-BDC NTs	**0.46**
Ni-BDC NTs	**0.61**
Ni_1Fe_1-BDC NTs	**1.32**
Ni_2Fe_1-BDC NTs	**3.8**
Ni_3Fe_1-BDC NTs	**0.59**
Ni_2Fe_1-BDC	**0.39**
RuO_2	**2.9**

Table S4. Overpotentials (10 mA cm^{-2}) of the recent reported MOF-based OER electrocatalysts in 1 M KOH.

Electrocatalyst	η_{10} (mV)	References
Ni_2Fe_1-BDC NTs	274	This work
S/N-CMF@FexCoyNi_{1-x-y}MOF	295	[1]
Ni-MOF@CNT	370	[2]
MCCF/NiMn-MOFs	280	[3]
NiCo-LDH-OH	317	[4]
CoNi-MOF	350	[5]
Ni-MOF	337	[6]
MIL@TA-Ni	282	[7]
$Fe(OH)_3$@Co-MOF-74	292	[8]
CoNi-MOF	310	[9]
CoPc@Co-MOF-74	291	[10]
Co-HAB-NSs	310	[11]
β-$Co(OH)_2$/Co-MOF	330	[12]
NiCoBi/NiCoMOF	317	[13]
Ni-Co-BTC	330	[14]
FeNi@CNF	356	[15]
Co-MOF	280	[16]

Table S5. Comparison of AEMWE performance paired with a Pt/C cathode.

Electrode	Temperature (°C)	Cell Voltage	Reference
Ni_2Fe_1-BDC NTs||Pt/C	60	1.72	This work
$Ni_{0.5}Co_{0.5}MoO_4 \bullet nH_2O$||Pt/C	50	1.82	[17]
Fe-$NiCo_2S_4$@NIF||Pt/C	RT	1.83	[18]
$Ni_{0.6}Co_{0.2}Fe_{0.2}$||Pt/C	50	1.87	[19]
$Fe_{10}Co_{45}Ni_{45}$ MOF||Pt/C	60	1.9	[20]
Ni_2P/Ni_7S_6||Pt/C	65	1.94	[21]
NiFe LDH-MoS_x/INF||Pt/C	60	1.95	[22]
$CoSb_2O_6$||Pt/C	60	1.98	[23]
Fe/S-NiOOH/NF||Pt/C	60	2.24	[24]

Reference

[1] Y. F. Zhao, X. F. Lu, Z. P. Wu, Z. H. Pei, D. Y. Luan and X. W. Lou, *Adv. Mater.*, 2023, **35**, 2207888.

[2] T. V. M. Sreekanth, G. R. Dillip, P. C. Nagajyothi, K. Yoo and J. Kim, *Appl. Catal. B-Environ. Energy*, 2021, **285**, 119793.

[3] W. R. Cheng, X. F. Lu, D. Y. Luan and X. W. Lou, *Angew. Chem. Int. Ed.*, 2020, **132**, 18391-18396.

[4] H. Yang, Z. H. Zhou, H. J. Yu, H. L. Wen, R. N. Yang, S. M. Peng, M. Sun and L. Yu, *J. Colloid Interface Sci.*, 2023, **636**, 11-20.

[5] S. K. Konavarapu, G. Kim, K. Shin and S. Y. Kim, *Chemistry-A European Journal*, 2025, **31**, e202500010.

[6] A. Patil, M. Samtham, E. Choudhary, A. Yadav, A. Miglani, S. Bimli, H. Jadhav and R. S. Devan, *Int. J. Hydrog. Energy*, 2025, **112**, 408-417.

[7] K. Ji, Y. L. Yue and P. Yang, Appl. Surf. Sci., 2023, **608**, 155184.

[8] Z. Gao, Z. W. Yu, F. Q. Liu, C. Yang, Y. H. Yuan, Y. Yu and F. Luo, *ChemSusChem*, 2019, **12**, 4623-4628.

[9] Q. C. Liu, J. H. Chen, P. Yang, F. Yu, Z. Y. Liu and B. H. Peng, *Int. J. Hydrog. Energy*, 2021, **46**, 416-424.

[10] J. Z. Jia, X. H. Zhao, W. H. Hu, Y. T .Wang, J. F. Huang, J. E. Huang, H. Li, Y. Peng, H. Y. Ma and C. L. Xu, *Int. J. Hydrog. Energy*, 2023, **11**, 8141-8149.

[11] C. Li, L. L. Shi, L. L. Zhang, P. Chen, J. W. Zhu, X. Wang and Y. S. Fu, *Int. J. Hydrog. Energy*, 2020, **8**, 369-379.

[12] J. Q. Wu, Z. H. Zhao, Y. W. Hua, Y. L. Wu, S.-Y. Ye, J. T. Qian, M. L. Li, L. W. Zhu, Z. Yan and X. Cao, *Inorg. Chem.*, 2023, **62**, 15641-15650.

[13] L. L. Zhao, M. Hong, X. H. Zhang, C. C. Du and J. H. Chen, *J. Alloy. Compd.*, 2025, **1016**, 179010.

[14] S. Singh, M. Yadav, D. K. Singh, D. K. Yadav, P. K. Sonkar and V. Ganesan, *New J. Chem.*, 2022, **46**, 13422-13430.

[15] Y. W .Li, M. T. Lu, P. P. He, Y. H .Wu, J. W. Wang, D. N. Chen, H. Xu, J. K. Gao and J. M. Yao, *Chem.-Asian J.*, 2019, **14**, 1590-1594.

[16] R. K. Tripathy, A. K. Samantara and J. N. Behera, *Dalton Trans.*, 2019, **48**, 10557-10564.

[17] A. Karmakar, T. G. Senthamaraikannan, E. Baasanjav, P. Bandyopadhyay, B. Jin, Y. Park, D.-H. Lim and S. M. Jeong, *Appl. Catal. B-Environ.*, 2023, **328**, 122504.

[18] F. L. Wang, Y. W. Dong, C. J. Yu, B. Dong, X. Y. Zhang, R. Y. Fan, J. Y. Xie, Y. N. Zhou and Y. M. Chai, *Appl. Catal. B-Environ. Energy*, 2023, **331**, 122660.

[19] A. Y. Faid, A. O. Barnett, F. Seland and S. Sunde, *Int. J. Hydrog. Energy*, 2022, **47**, 23483-23497.

[20] A. Abdelhafiz, M. H. Mohammed, J. Abed, D. C. Lee, M. Chen, A. S. Helal, Z. Ren, F. Alamgir, E. Sargent, P. A. Kohl, S. K. Elsaidi and J. Li, *Adv. Energy Mater.*, 2024, **14**, 2303350.

[21] F. L. Wang, N. Xu, C. J. Yu, J. Y. Xie, B. Dong, X. Y. Zhang, Y. W. Dong, Y. L. Zhou and Y. M. Chai, *Appl. Catal. B-Environ. Energy*, 2023, **330**, 122633.

[22] H. Zhang, G. Q. Shen, X. Y. Liu, B. Ning, C. X. Shi, L. Pan, X. W. Zhang, Z. F. Huang and J. J. Zou, *Chin. J. Catal.*, 2021, **42**, 1732-1741.

[23] K. Ham, S. Hong, S. Kang, K. Cho and J. Lee, *ACS Energy Lett.*, 2021, **6**, 364-370.

[24] F. L. Wang, J. L. Tan, Z. Y. Jin, C. Y. Gu, Q. X. Lv and Y. W. Dong, R. Q. Lv, B. Dong, Y. M. Chai, *Small*, 2024, **20**, 2310064.